Int J Adv Manuf Technol (2014) 73:805–819
DOI 10.1007/s00170-014-5832-5

ORIGINAL ARTICLE

# Three-dimensional precision analysis with rigid and compliant motions for sheet metal assembly

**Jun Ni · Wencheng Tang · Yan Xing**

Received: 24 January 2013 / Accepted: 1 April 2014 / Published online: 9 May 2014


**Abstract** This paper quantifies the detailed assembly motions by taking into account the mating gaps and gravities of fixtures and sheet metals. Finite element (FE) models are firstly generated for fixtures and parts. Their nodes are ordered according to an appointed assembly sequence where the last assembled part is behind the first one by the assembly platform or mating surface. Three noncollinear feature points are selected from each last assembled part near the mating surface. Their translational displacements (gaps) represent the part rigid motion near that surface omitting the local joint deformation. Based on the given feature point gaps, kinematic formulations are proposed to compute the rigid motions for any FE nodes behind the mating surface in assembly sequence. Compliant motions are then reached by the modified FE analysis where variable mesh method is applied to change the FE nodal coordinates using the gap-induced rigid motions and deformations. Code integrations of sequence and parallel assemblies are finally proposed and validated via simulations and experiments. Results suggest the following: (1) the proposed method is effective and accurate for engineer application; (2) the integration approach requires to be further studied for the precision analysis of more complex assemblies and implies a feasible way for adding local deformations of joints to the deterministic dimensional precision analysis.

**Keywords** Sheet metal · Assembly · Three-dimensional · Rigid motion · Compliant motion

J. Ni (✉) · W. Tang (✉) · Y. Xing (✉)
School of Mechanical Engineering, Jiulong Lake Campus, Southeast University, Nanjing 211189, People's Republic of China
e-mail: juuuuny@live.cn
e-mail: tangwc@seu.edu.cn
e-mail: xingyan@seu.edu.cn

## 1 Introduction

Sheet metals form the framework of precision industrial products, e.g., aircraft, radar, vehicle, and so on. Fatigue tolerance and global deformation of the products are affected by the joints inside [1, 2]. Electronic performance of large-scale radar directly relates to the framework shape which is actually deviated from the theoretical shape by assembly dimensional variations [3, 4]. Product dimensional precision control requires formulating the deterministic quantitative relation between the global deformation distribution and the dimensional error sources, i.e., geometric error, mating gaps (fixture-to-part locating error and part-to-part locating error), joint deformation, and gravity. Then, stochastic statistical models of the error sources will start further probability analysis based on the deterministic relation.

Part geometric error is well considered by the tolerance analysis and allocation using stochastic models such as probability density function, fuzzy membership function, and the worst case estimation [5]. The recent tolerance analysis platform integrates finite element (FE) analysis module and statistical analysis tool into optimization software, which provides the tolerance analysis with the capability of accommodating the effects of contact force and acceleration [6]. To handle the influence of fixture-to-part locating errors and multistage processes, several techniques, which advance the dimensional variation analysis and fixture layout design, have been proposed especially for the automotive assembly.

Stream-of-Variation Analysis (SOVA) is as compared to the $6\sigma$ probability analysis based on a deterministic relationship that relates error sources to global deformation [7, 8]. In influence coefficient method, the linear relation between fixture-to-part locating error vector and elastic deformation vector gives born to the Compliant Assembly Variation Analysis software

using FE analysis [9]. From the point of view of fixture, "*N*-2-1" layout is developed from the "3-2-1" layout of rigid body, and the FE analysis is used for the optimization of *N* [10]. Research efforts in compliant digital panel assemblies also evolve software package Elastic Assembly Variation Simulation (EAVS). Then, rivet joint deformation and part-to-part contact behavior are focused. (1) Interpolate the tested local riveting deformation to FE deformation result of EAVS [11]. (2) Based on EAVS, the nonlinear contact behavior and two numerical probability solutions are discussed [12]. And (3) the contact behavior is added to the influence coefficient method [13]. In the above methods, the deterministic relation obeys force closure.

On the other hand, form closure lies in the methods using kinematic balance with 3-2-1 fixture layout. The form closure-based analytical and numerical solutions of part resultant translational and/or orientation errors due to part geometric errors and/or fixture-to-part errors are comprehensively studied for the fixture layout design [14]. The transfer mechanism of three-dimensional (3D) rigid variation is also studied for the multistage process [15]. State space method is proposed to handle the influence factors of the rigid motions in multistage assembly such as lap joints, fixture errors, and mating gaps between fixture and part [16]. The state space method drives many control researches for the variation analysis, design, and diagnosis [17].

At the system level, the product-oriented sensitivity analysis model and the two-step linear model are, respectively, developed from force closure and form closure models [18, 19]. On the contrary, the aforementioned models are limited for the detailed variation analysis and consider either mating feature or fixture.

To deal with this challenge, a 3D rigid SOVA model that considers both the fixture and mating feature is proposed for the multistages assembly [20, 21]. Then, its capabilities are extended by enabling the geometric error via adding a statistical modal analysis [22]. Meanwhile, many efforts can be included from the point of view of compliant assembly. (1) A variation propagation model that considers the part deformation due to various joining and releasing schemes is proposed for the use at the preliminary design phase [23]. (2) Three submodels are combined into a deterministic detailed relation considering the error sources in a riveting process, and then finish a probability analysis by Monte Carlo simulation [24].

Either form closure- or force closure-based method cannot be easily extended to detailed dimensional precision analysis for the compliant assembly considering both the mating feature and fixture. In [25], the fixture layout design method for minimizing the translational and orientational variations of key points in the sheet panels is extended from a form closure-based robust design approach. This work implies an opportunity using kinematic formulation for the compliant assembly. In light of this opportunity, we attempt to find a methodology combining the rigid closure and force closure properties for the comprehensive dimensional precision analysis of complaint assembly. Hence, the over constraint effect is added to the generic rigid assembly process studied in [20].

From the assembly process, positioning, clamping, and releasing are focused, while joining is studied in the other paper [26]. Clamps are removed after assembly, so they are only considered in related experiments. Because clamping and joining are neglected by simulation, over constraint only occurs when involving either the gravity or the two groups of mating gaps (one mating surface one group) or both. It also means every mating surface is full constrained. Thus, rigid motion that is induced by mating gaps (gap-induced rigid motion) is more obvious at the part region near mating surface. In contrary, complaint motion is more obvious at the other regions, i.e., gravity and/or gap-induced deformations.

We assume the three types of motions can be linearly stacked. In this paper, kinematic formulations are established based on an approximation of velocity to micro motion; then, positions of the related regions in fixtures and/or parts are modified by the rigid motions solved by kinematic formulations; finally, a FE analysis integrated approach adds the gravity and/or gap-induced deformations. The entire approach benefit is the comprehensive dimensional precision analysis that constitutes a sound basis for the participation of joint distortions, and further probability analysis and process optimization with the purpose to improve dimensional precision of compliant assembly.

The following paragraphs are organized as follows. Section 2 introduces the generic assembly process and announcements. Section 3 proposes the kinematic formations for the gap-induced rigid motion. Section 4 presents the FE analysis integrated approach for calculating the compliant motion and the specific steps for the dimensional precision analysis of sequence and parallel assemblies. Section 5 shows the performance of the proposed method through simulations and experiments. Section 6 draws the conclusion and future work.

## 2 A generic assembly process and announcement

The generic assembly process in [20] is modified as the follows.

- Based on the assembly platform, fixtures and parts are positioned and clamped sequentially to the root part.
- In assembly sequence, last assembled part is behind the first one by their mating surface that is considered as a surface belonging to the last part.

- The resulting subassemblies will form new root parts.
- Root parts are full constrained or over constrained.
- The other parts are positioned by either part-to-part or part-to-fixture mating surfaces or both.

Assumptions are the following: (1) Geometric error and joint distortion are neglected. (2) Part-to-part and fixture-to-part mating gaps are so smaller that they can be represented by micro velocities. (3) Gap-induced rigid motion, gap-induced deformation, and gravity-induced deformation can be linearly stacked. (4) Fixtures and parts are represented by the discrete nodes of FE models.

The following introduces the unified 3D motion description, the selected points for dimensional precision analysis, and the related coordinate conversion.

### 2.1 3D motion description

Rigid motion is well described by three pairs of translational and rotational displacements, i.e.,

$$\Delta\overrightarrow{P} = [\delta x, \delta y, \delta z, \delta\alpha, \delta\beta, \delta\gamma]^T.$$

The pitch of each pair relates rotation about one axis to translation along that axis. Figure 1 illustrates this geometric meaning. Also, three noncollinear points in Fig. 1 can represent the rigid motion. The minimized form is:

$$\Delta\overrightarrow{P} = [\delta x_1, \delta y_1, \delta z_1, \delta y_2, \delta z_2, \delta z_3]^T. \quad (1)$$

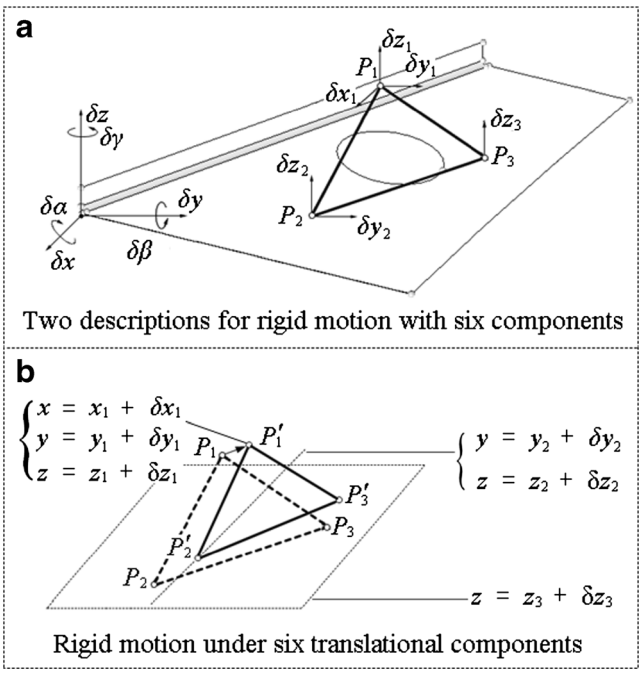


**Fig. 1** Rigid motion description. **a** Two descriptions for rigid motion with six components; **b** Rigid motion under six translational components

*Proof*

- The rigid part can be represented by any plane in the part.
- Due to three noncollinear points determine one plane, three points are sufficient for the part representation, i.e., $\left[\Delta\overrightarrow{P}_1^T, \Delta\overrightarrow{P}_2^T, \Delta\overrightarrow{P}_3^T\right]^T$.
- As shown in Fig. 1, rigid part means the lengths and angles of the triangle formed by $P_1$, $P_2$, and $P_3$ will not change. It yields Eq. 2, where $i, j$, and $k$, respectively, take 1, 2, 3, and $P_1'$, $P_2'$, $P_3'$ are the new position points for $P_1$, $P_2$, and $P_3$ after a rigid motion.

$$\begin{cases} \left|\overrightarrow{P_iP_j}\right| = \left|\overrightarrow{P_i'P_j'}\right| \\ \left|\overrightarrow{P_iP_j} \times \overrightarrow{P_iP_k}\right| = \left|\overrightarrow{P_i'P_j'} \times \overrightarrow{P_i'P_k'}\right| \end{cases}. \quad (2)$$

- If the rigid motion takes the smallest value, the other components of $\left[\Delta\overrightarrow{P}_1^T, \Delta\overrightarrow{P}_2^T, \Delta\overrightarrow{P}_3^T\right]^T$ can be determined by the substitution of components ($\delta x_1$, $\delta y_1$, $\delta z_1$, $\delta y_2$, $\delta z_2$, and $\delta z_3$) into Eq. 2. Proof of Eq. 1 is finished.

Because the representation of part deformation requires the translational displacements of a series of points, e.g., the discrete nodes in their FE models, the unified motion description prefers the translational displacements of selected points which at least contain three noncollinear points.

### 2.2 The used point announcement

Key and feature points are selected from the FE nodes or experimental sample. A series of key points locate at the place where the assembly motion is concerned. Three noncollinear feature points locate at the last assembled part near the mating surface.

Mating gaps at the feature points are the displacement increments causing micro rigid motion of the assembled part, i.e., the main character of mating feature. Three pairs of deterministic gaps at the feature points imply that the part is full constrained while the part that has more is over constrained.

For each mating feature, the positions and mating gaps of feature points can be converted to the position and motion of one reference point. The merit of reference point is quickly spreading the influence of mating gaps to the other place behind the mating surface in the assembly sequence, which is shown in Section 3.

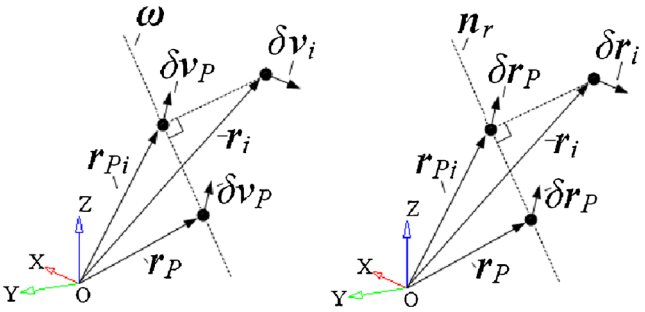


**Fig. 2** Relation of rotational motions

### 2.3 Coordinate conversion

Global coordinate system (GCS) is fixed on the assembly platform.

Local coordinate system (LCS) which origin coincides with the reference point is defined for each mating feature.

Mating gaps possible with stochastic models are assumed or measured in the LCS. If part rotations obey the order *z*-*x*-*y*, the coordinate transformation satisfies

$$\overrightarrow{R} = A\overrightarrow{r} + \overrightarrow{P}_r,$$

where ***R***, ***r*** are the feature point vectors in GCS and LCS, respectively. ***Pr*** is the reference point vector in GCS and coordinate conversion transfer matrix

$$A = \begin{bmatrix} \cos\gamma_P & -\sin\gamma_P & \\ \sin\gamma_P & \cos\gamma_P & \\ & & 1 \end{bmatrix} \begin{bmatrix} 1 & & \\ & \cos\alpha_P & -\sin\alpha_P \\ & \sin\alpha_P & \cos\alpha_P \end{bmatrix} \begin{bmatrix} \cos\beta_P & & \sin\beta_P \\ & 1 & \\ -\sin\beta_P & & \cos\beta_P \end{bmatrix}.$$

No matter where the LCS origin is, motion satisfies $\delta\overrightarrow{R} = A\delta\overrightarrow{r}$ .

## 3 Rigid motion calculation for one mating feature

Given the mating gaps in the form of (1) in LCS, the whole gap vectors, $\delta\boldsymbol{r}_1$, $\delta\boldsymbol{r}_2$, $\delta\boldsymbol{r}_3$, can be solved according to the proof of (1).

If $\delta\boldsymbol{r}_1$, $\delta\boldsymbol{r}_2$, and $\delta\boldsymbol{r}_3$ are the same vector, the part is on a translation. The motion vector equates to $\delta\boldsymbol{r}_1$.

Otherwise, the part motion at most comprises three screw motions along three independent axes. The main motion is focused because it has a little probability that more than one screw motion can occur with the same weight, and the motion is very tiny compared to the part dimensions. It means that the part is on a transient screw motion, i.e., one pitch relates micro rotation about a fixed axis to micro translation along that axis. If the reference point is selected on that axis, [27] suggests any point motion and the reference point motion satisfy

$$\begin{bmatrix} \delta x_j & \delta y_j & \delta z_j & \delta\alpha_j & \delta\beta_j & \delta\gamma_j \end{bmatrix}^T = \begin{bmatrix} I & Q_{jr} \\ & I \end{bmatrix} \begin{bmatrix} A & \\ & A \end{bmatrix} \Delta\overrightarrow{P}_r,$$

where $I$ is a 3×3 identity matrix, $j$ is the identity number of point $(x_j, y_j, z_j)$ in GCS, $r$ is the reference point label, and $Q_{jr}$ satisfies in Eq. 3.

$$Q_{jr} = \begin{bmatrix} 0 & z_j - z_r & y_r - y_j \\ z_r - z_j & 0 & x_j - x_r \\ y_j - y_r & x_r - x_j & 0 \end{bmatrix}. \tag{3}$$

Because translational displacements of a series of points are efficient for the rigid motion expression, the equation between any point motion and reference point motion can be reduced as:

$$\begin{bmatrix} \Delta x_j, \Delta y_j, \Delta z_j \end{bmatrix}^T = \begin{bmatrix} I & Q_{jr} \end{bmatrix} \Delta\overrightarrow{P}_r. \tag{4}$$

Equations 3 and 4 will give 3D rigid motion to any part nodes behind the mating surface. Thus, determining the position and motion of reference point is focused.

### 3.1 Derivation of the rotational component for rigid motion

The known variables are mating gaps ($\delta\boldsymbol{r}_1$, $\delta\boldsymbol{r}_2$, and $\delta\boldsymbol{r}_3$), feature point positions ($\boldsymbol{r}_1$, $\boldsymbol{r}_2$, and $\boldsymbol{r}_3$). Due to the displacement differentiation is velocity, transient micro motions can be considered as velocities. Figure 2 shows the velocity relation where $\overrightarrow{n}_r$ is angular velocity, $\overrightarrow{r}_i - \overrightarrow{r}_{Pi}$ is rotational radius,

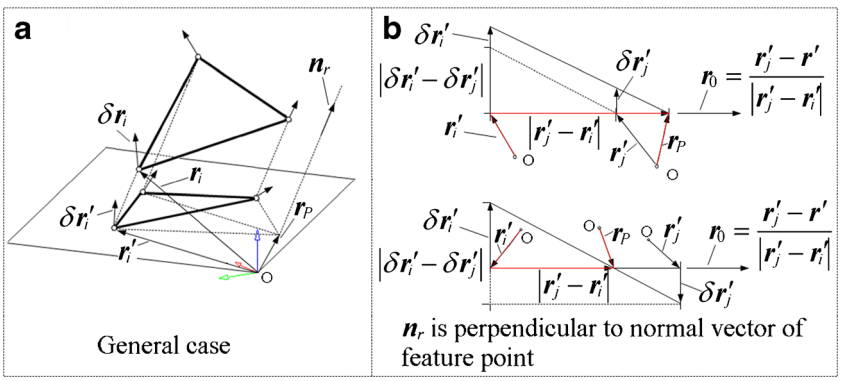


**Fig. 3** Determination of one reference point position by vector projections of feature point positions and gaps. **a** General case; **b** $n_r$ is perpendicular to the normal direction of feature point plane

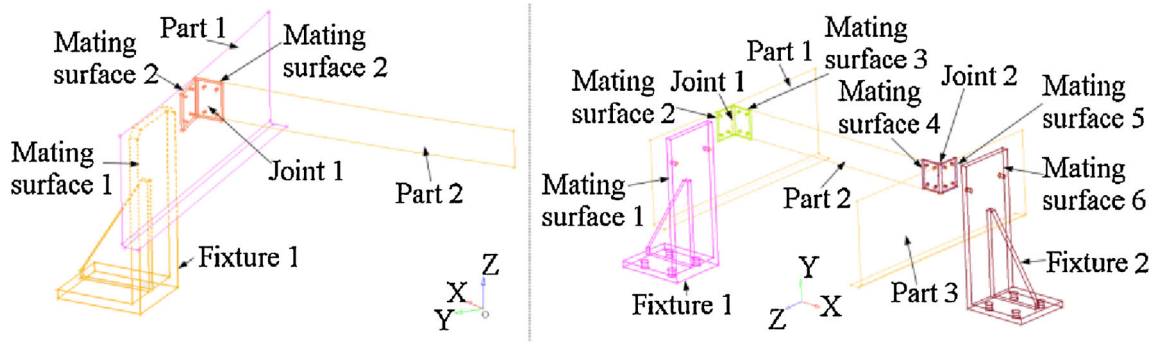


**Fig. 4** 3D forms for the sequence and parallel assemblies

$\delta\vec{r}_p$ is the translation along axis, and $A\delta\vec{r}_i$ is rotational velocity in GCS. For three feature points, Eqs. 5 and 6 hold.

$$\begin{cases} \vec{n}_r \times (\vec{r}_1 - \vec{r}_{P1}) + \delta\vec{r}_p = A\delta\vec{r}_1 \\ \vec{n}_r \times (\vec{r}_2 - \vec{r}_{p2}) + \delta\vec{r}_p = A\delta\vec{r}_3 \\ \vec{n}_r \times (\vec{r}_3 - \vec{r}_{P3}) + \delta\vec{r}_p = A\delta\vec{r}_3 \end{cases}. \tag{5}$$

$$\begin{cases} \vec{r}_{P1} = \vec{r}_P + k_1\vec{n}_r \\ \vec{r}_{P2} = \vec{r}_P + k_2\vec{n}_r \\ \vec{r}_{P3} = \vec{r}_P + k_3\vec{n}_r \end{cases}. \tag{6}$$

Use Eq. 6 to eliminate $\vec{r}_{Pi}$ in Eq. 5. Subtract different equations in Eq. 5 with subscript taking one feature point number, e.g., $i$ or $j$. Thus, Eq. 7 will be reached.

$$\vec{n}_r \times \left(\vec{r}_i - \vec{r}_j\right) = A\left(\delta\vec{r}_i - \delta\vec{r}_j\right), \tag{7}$$

where

$$\vec{n}_r = [\delta\alpha_P, \delta\beta_P, \delta\gamma_P]^T.$$

Because

$$\vec{r}_i - \vec{r}_j = \left[x_i - x_j, y_i - y_j, z_i - z_j\right]^T,$$

Eq. 7 equates to

$$Q_{ij}\vec{n}_r = A\left(\delta\vec{r}_i - \delta\vec{r}_j\right), \tag{8}$$

where $Q_{ij}$ satisfies (Eq. 3) with subscript $r$ replaced by $j$. The least square solution of Eq. 8 gives the rotational component

$$\vec{n}_{r3\times 1} = \begin{bmatrix} Q_{12} \\ Q_{23} \\ Q_{31} \end{bmatrix}^+_{9\times 3} \begin{bmatrix} A(\delta\vec{r}_1 - \delta\vec{r}_2) \\ A(\delta\vec{r}_2 - \delta\vec{r}_3) \\ A(\delta\vec{r}_3 - \delta\vec{r}_1) \end{bmatrix}_{9\times 1}. \tag{9}$$

### 3.2 Derivation of the position and motion for reference point

A projection plane that is perpendicular to $\boldsymbol{n}_r$ is defined through the GCS origin.

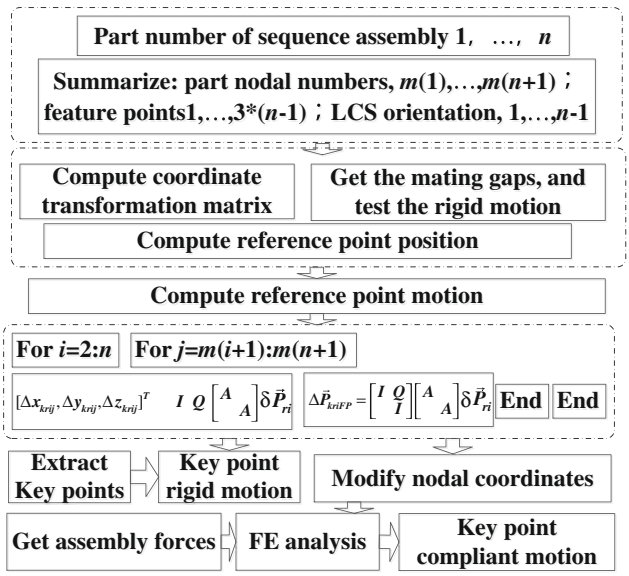


**Fig. 5** 3D motion calculation process for the sequence assembly

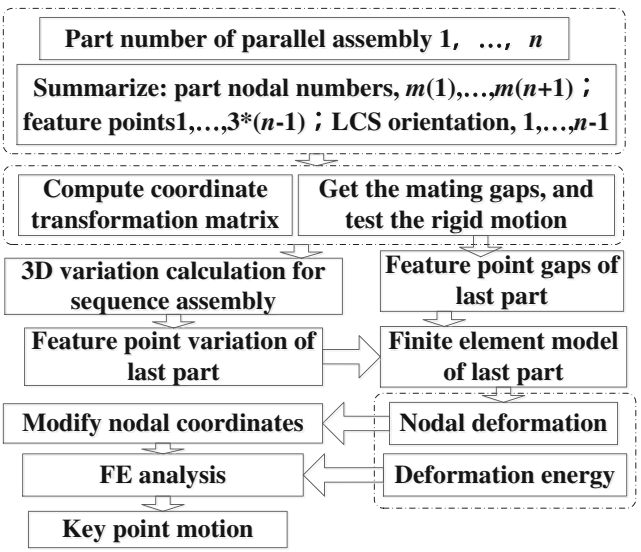


**Fig. 6** 3D motion calculation process for the parallel assembly

Equations 10 and 11, respectively, give the projections of position and gap vectors for feature point *i*.

$$\vec{r}_i' = \vec{r}_i - \left(\vec{r}_i \cdot \vec{n}_{r0}\right)\vec{n}_{r0}, \tag{10}$$

$$\delta\vec{r}_i' = A\delta\vec{r}_i - (A\delta\vec{r}_i \cdot \vec{n}_{r0})\vec{n}_{r0}, \tag{11}$$

where $\vec{n}_{r0} = \vec{n}_r / |\vec{n}_r|$ . The normal vector of feature point plane is given by:

$$\vec{n}_{FP} = \overrightarrow{P_iP_j} \times \overrightarrow{P_iP_k}. \tag{12}$$

Case 1. $\vec{n}_{FP}$ is not perpendicular to $\boldsymbol{n}_r$.

As shown in Fig. 3a, reference point is the common point of three lines which are vertical to the projections of feature point gap vectors. It yields

$$\begin{cases} \vec{r}_P = \vec{r}_1' + k_1\left(\delta\vec{r}_1' \times \vec{n}_r\right) \\ \vec{r}_P = \vec{r}_2' + k_2\left(\delta\vec{r}_2' \times \vec{n}_r\right) \\ \vec{r}_P = \vec{r}_3' + k_3\left(\delta\vec{r}_3' \times \vec{n}_r\right) \end{cases}. \tag{13}$$

Equation 13 yields the solution of coefficients $k_1$, $k_2$, and $k_3$.

$$\begin{Bmatrix} k_1 \\ k_2 \\ k_3 \end{Bmatrix}_{3\times 1} = \begin{bmatrix} -\delta\vec{r}_1' \times \vec{n}_r & \delta\vec{r}_2' \times \vec{n}_r & 0 \\ 0 & -\delta\vec{r}_2' \times \vec{n}_r & \delta\vec{r}_3' \times \vec{n}_r \\ \delta\vec{r}_1' \times \vec{n}_r & 0 & -\delta\vec{r}_3' \times \vec{n}_r \end{bmatrix}^{+}_{9\times 3} \begin{Bmatrix} \vec{r}_1' - \vec{r}_2' \\ \vec{r}_2' - \vec{r}_3' \\ \vec{r}_3' - \vec{r}_1' \end{Bmatrix}_{9\times 1} \tag{14}$$

The position vector of reference point is determined by the substitution of Eq. 14 into Eq. 13.

Case 2. $\vec{n}_{FP}$ is perpendicular to $\boldsymbol{n}_r$.

As expressed by Fig. 3b, projection vectors of $\delta\boldsymbol{r}_1$, $\delta\boldsymbol{r}_2$, and $\delta\boldsymbol{r}_3$ are paralleled to each other. The position vector of reference point is determined by

$$\vec{r}_P = \vec{r}_i' + \frac{|\delta\vec{r}_i'|}{|\delta\vec{r}_i' - \delta\vec{r}_i'|}\left(\vec{r}_j' - \vec{r}_i'\right). \tag{15}$$

Dot product between one of the three feature point position vectors and the unit rotational axis vector targets at a same vector, i.e., the micro translation along this axis,

$$\delta\vec{r}_P = \left(A\delta\vec{r}_i \cdot \vec{n}_{r0}\right)\vec{n}_{r0}.$$

Hence, the reference point motion vector satisfies

$$\Delta\vec{P}_{ri} = \left[\left(A\delta\vec{r}_j \cdot \vec{n}_{r0}\right)\vec{n}_{r0}^{\,T}, \vec{n}_r^{\,T}\right]^T. \tag{16}$$

**Table 1** Material property for the assembly

| Part | Material | Density | Young's modulus | Poisson ratio |
|---|---|---|---|---|
| Sheet metals | 2A05 Al | 2.65 g/cm$^3$ | 70GPa | 0.32 |
| Fixtures | Q235 Fe | 7.8 g/cm$^3$ | 200GPa | 0.33 |

## 4 Rigid and compliant motions integration method

According to the assembly sequence, visit the mating surface one by one starting from one fixture and do Step 1 to Step 3 until a part that has three more feature points is met (over-constraint).

- Step 1. Use the positions and motions of three feature points to calculate the reference point position and motion by Eqs. 9, 13–16.
- Step 2. Use Eqs. 3 and 4 to calculate the rigid motions for any FE nodes which are behind the mating surface.
- Step 3. Add the solved rigid motions into the related FE nodal coordinates by variable mesh method.

If a part that has three more feature points is met, add the solved rigid motions of feature points to their mating gaps. Once all the mating gaps of the feature points of the part are updated, the "over-constraint" case

**Table 2** The LCS orientation of each part in GCS (unit; rad)

| *n* | Part | $\alpha_P$ | $\beta_P$ | $\gamma_P$ |
|---|---|---|---|---|
| 0 | Fixture 1 | 0 | π/2 | 0 |
| 1 | Part 1 | 0 | 0 | 0 |
| 2 | Joint 1 | 0 | 0 | 0 |
| 3 | Part 2 | 0 | 0 | π/2 |
| 4 | Joint 2 | 0 | 0 | 0 |
| 5 | Part 3 | 0 | 0 | 0 |
| 6 | Fixture 2 | 0 | π/2 | 0 |

**Table 3** The assumed gaps of the feature points near the mating surfaces in LCS (unit; mm)

| *n* | Name | Vector | Feature points | $\delta x$ | $\delta y$ | $\delta z$ |
|---|---|---|---|---|---|---|
| 1 | Part 1 | $\vec{v}_1$ | $P_{11}$ | 2.659 | −2.657 | 0.1877 |
| | | | $P_{12}$ | | −0.9955 | 0.2169 |
| | | | $P_{13}$ | | | −1.905 |
| 2 | Joint 1 | $\vec{v}_2$ | $P_{21}$ | 0.3333 | 0.3333 | 0.3333 |
| | | | $P_{22}$ | | 0.3333 | 0.3333 |
| | | | $P_{23}$ | | | 0.3333 |
| 3 | Part 2 | $\vec{v}_3$ | $P_{31}$ | 0.3333 | 0.3333 | 0.3333 |
| | | | $P_{32}$ | | 0.3333 | 0.3333 |
| | | | $P_{33}$ | | | 0.3333 |
| | | $\vec{v}_4$ | $P_{34}$ | 0.3333 | 0.3333 | 0.3333 |
| | | | $P_{35}$ | | 0.3333 | 0.3333 |
| | | | $P_{36}$ | | | 0.3333 |
| 4 | Joint 2 | $\vec{v}_5$ | $P_{41}$ | 0.3333 | 0.3333 | 0.3333 |
| | | | $P_{42}$ | | 0.3333 | 0.3333 |
| | | | $P_{43}$ | | | 0.3333 |
| 5 | Part 3 | $\vec{v}_6$ | $P_{51}$ | 0.3333 | 0.3333 | 0.3333 |
| | | | $P_{52}$ | | 0.3333 | 0.3333 |
| | | | $P_{53}$ | | | 0.3333 |

will be handled by one FE analysis where the gravity can also be involved.

Both the rigid motion calculation and the variable mesh codes are programmed in FORTRAN where FE analysis codes are integrated. To indicate the integration approach for the generic precision analysis codes, classic sequence and parallel assemblies used in [7] are extended to the 3D forms in Fig. 4. Fixture, part, and mating surface names are labeled. The horizontal assembly platform where fixtures are located is not shown.

### 4.1 3D motion calculation process for sequence assembly

The motion calculation process for the sequence assembly is given in Fig. 5. All parts are ordered from 1 to *n* according to the assembly sequence, e.g., Fixture 1, Part 1, Joint 1, and Part 2. Feature points are grouped and numbered according to the mating surfaces and the belongings to related parts.

Array *m* records the accumulated numbers of the related FE nodes in the assembly sequence. $m(1)$ is set to 0. $m(i)$ records

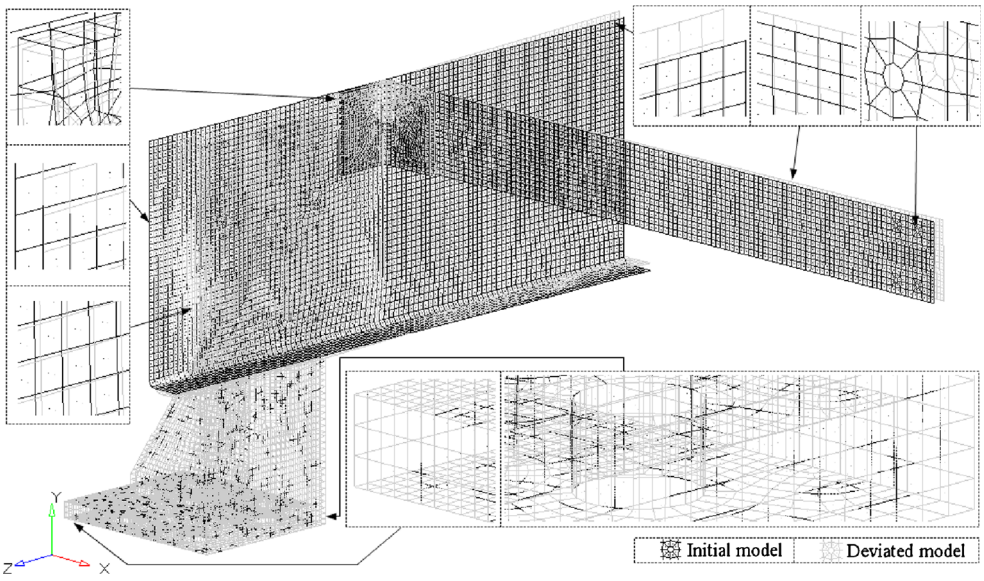


**Fig. 7** 3D rigid motion of sequence assembly

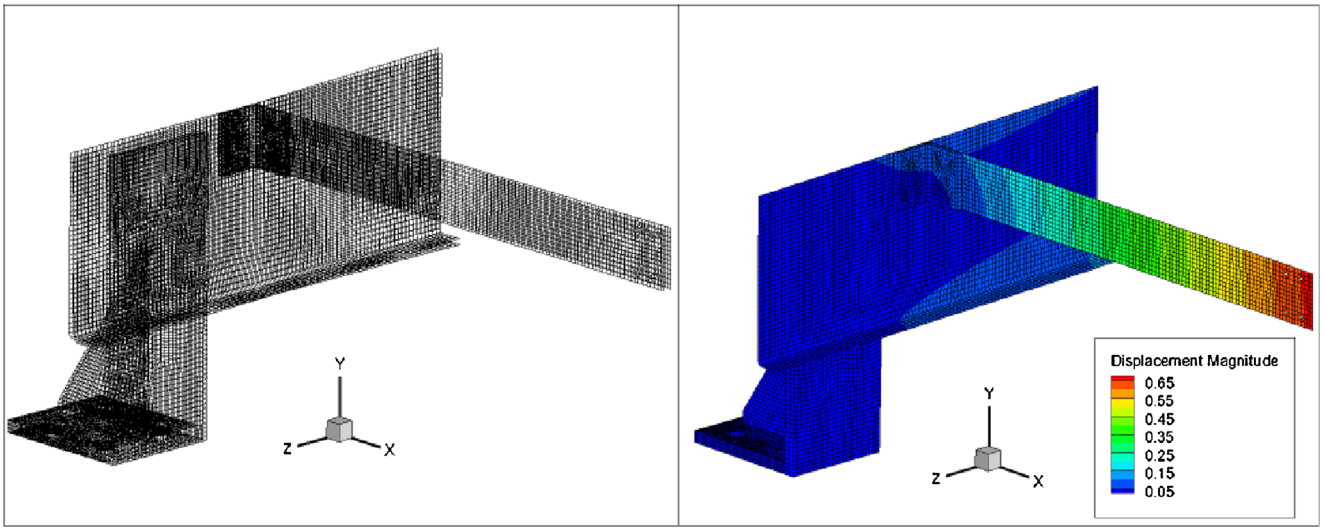


**Fig. 8** 3D motion of the sequence assembly (unit, mm)

the total node number before part $i$ with $i$ taking 2 to $n$+1. This array guarantees visiting the required part nodes in FE codes.

Thus, two iterations can determine the 3D rigid motions for the FE nodes behind the mating surface. After all the mating gaps are considered, one FE analysis can add the gravity-induced motion for the sequence assembly.

### 4.2 3D motion calculation process for parallel assembly

The motion calculation process for the parallel assembly is shown in Fig. 6. Fixtures and parts in the right chart of Fig. 4 contain two sequences. One is Fixture 1, Part 1, and Joint 1. And the other is Fixture 1, Part 3, and Joint 2. They are paralleled to the last part, Part 2.

The gap-induced rigid motions for sequence assemblies and the rigid motions of feature points for Part 2 can be solved by the rigid motion calculation method.

Then, the gap- and gravity-induced deformations are calculated as follows.

- Apply the rigid motions and mating gaps to the feature points of Part 2 as the boundary condition.
- Finish the FE analysis of Part 2.

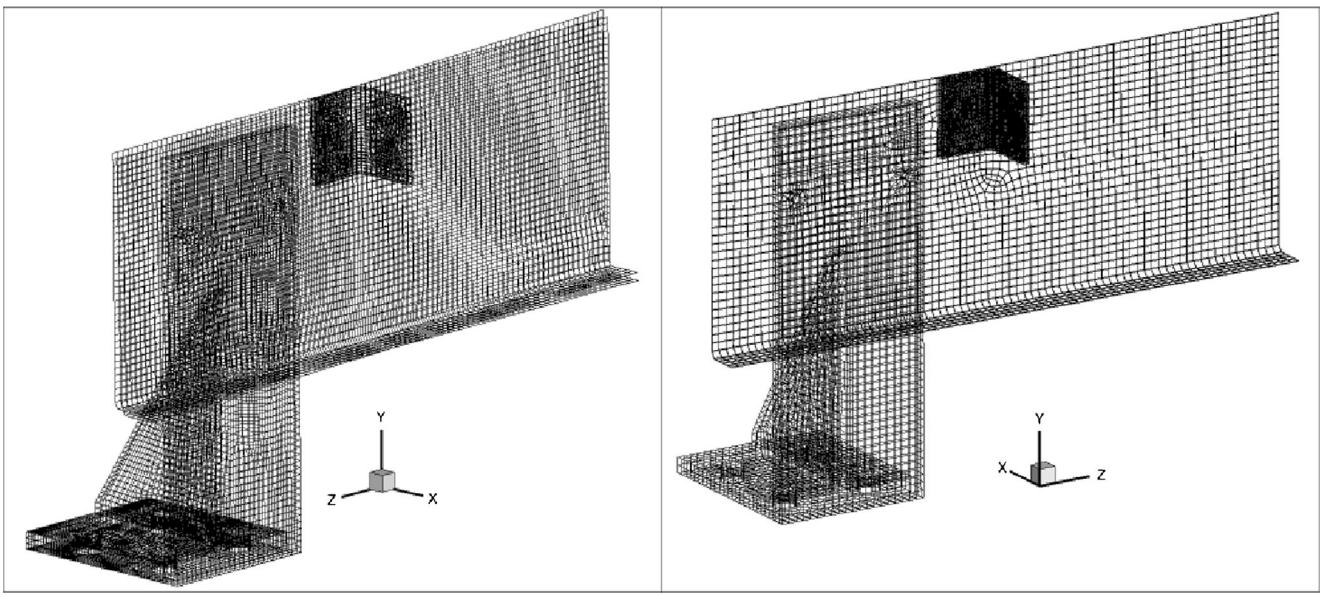


**Fig. 9** 3D rigid motion of two group sequential parts in the parallel assembly

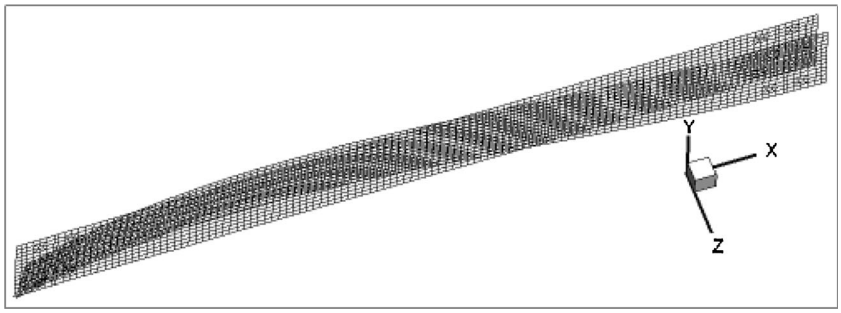


**Fig. 10** Gap-induced deformation of Part 2 in the parallel assembly

- From the FE analysis result, output the reacting forces at the feature points and every nodal deformations of Part 2.
- Apply the variable mesh method to modify the FE nodal coordinates using the nodal deformations for Part 2. Because the deformations are micro displacements, the variable mesh method will not trigger mesh distortion.
- Compute the deformation for the entire assembly based on the modified FE model with the reacting forces and gravity.

## 5 Simulation and experiment validations

To show the method performance, validations comprise two aspects. One is the simulations with assumed gaps for sequence and parallel assemblies. The other performs a comparison between the simulated and tested results based on two experiments with different clamps.

### 5.1 Simulation validation

The rigid motion calculation method and 3D motion calculation processes are, respectively, validated. The former uses sequence assembly. The latter uses both the assemblies in Fig. 4.

Their FE models are firstly generated. In the FE models, fixtures use solid elements; sheet metals use shell elements; the detailed joints are replaced by rigid beam elements; the bottom of fixtures is full constrained; and gravity is applied along the negative direction of axis *Y* of GCS. Table 1 lists the material property.

The parallel assembly has more parts than sequence assembly, i.e., the added Joint 2, Part 3, and Fixture 3. So, their information is given together. Feature points are selected from the FE nodes of every last assembled parts near mating surfaces. The LCS orientations and mating gaps are, respectively, given in Tables 2 and 3. $\overrightarrow{v}_1$ in Table 3 is a rotational gap vector while the others are translational gap vectors.

#### *5.1.1 3D rigid motion calculation result*

Figure 7 directly shows the rotation and translation which are calculated by Eqs. 4 and 16 using the rigid motion calculation method. The local amplified charts can also be found in Fig. 7. It shows the different motion forms at different places.

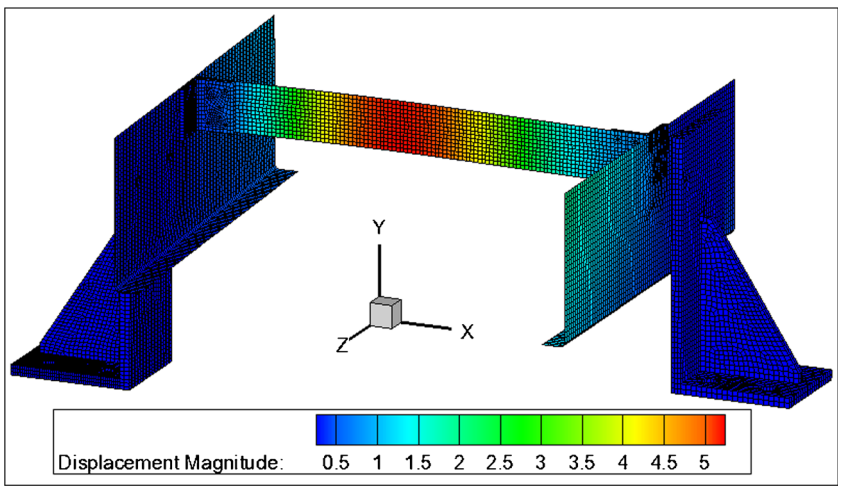


**Fig. 11** The released deformation of the parallel assembly (unit, mm)

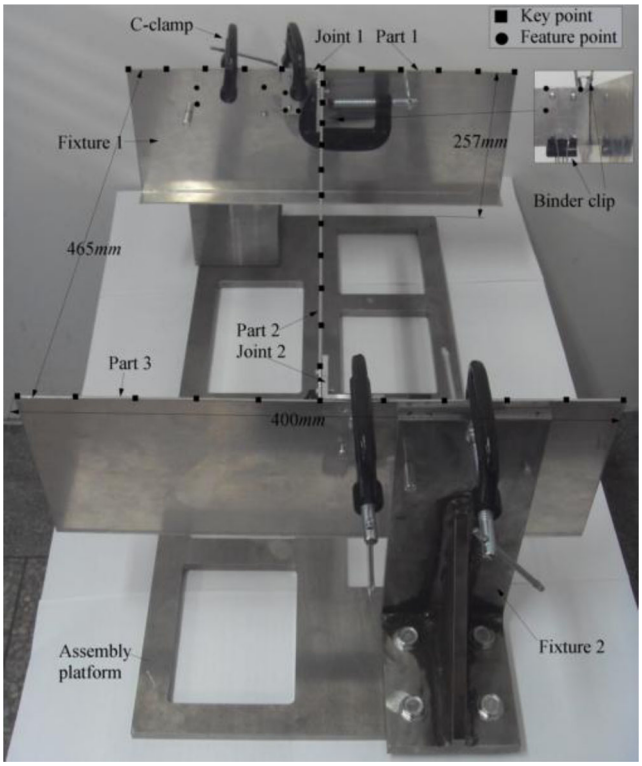


**Fig. 12** Main dimensions and point locations in the test sample

### 5.1.2 Results of 3D precision analysis with rigid and compliant motions

Figure 8 shows the mesh comparison before and after the rigid motion, and the final 3D motion of the sequence assembly. Figures 9 and 10 display the gap-induced motion of the parallel assembly while the released deformation of the modified FE model for the entire assembly is shown in Fig. 11.

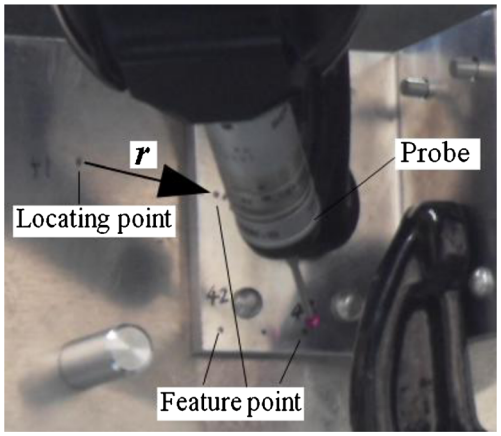


**Fig. 14** Locating point of each three feature points

### 5.1.3 Discussion about the simulation results

In Section 5.1.1, rigid motion is calculated from Eq. 4 to Eq. 16. The root mean square (RMS) error estimation for Eq. 16 is given by Eq. 17. It can be easily derived from Eq. 8, so the derivation is not shown.

$$E_{rms} = \frac{1}{C_3^2} \sum_{i = 1,\ldots,3; j = 1,\ldots,3; i \neq j} \left| \vec{n}_r \times \left( \vec{r}_i - \vec{r}_j \right) - A\left( \delta\vec{r}_i - \delta\vec{r}_j \right) \right|. \tag{17}$$

The RMS error for the rigid motion is 0.02590 mm. Compared to the smallest motion magnitude 0.3333 mm, it is deviated by 7 %. So, Eq. 16 has enough precision for further application. The precision of the entire approach relates to the FE analysis error and rigid motion calculation error. Because these errors are very small, the entire approach is accurate.

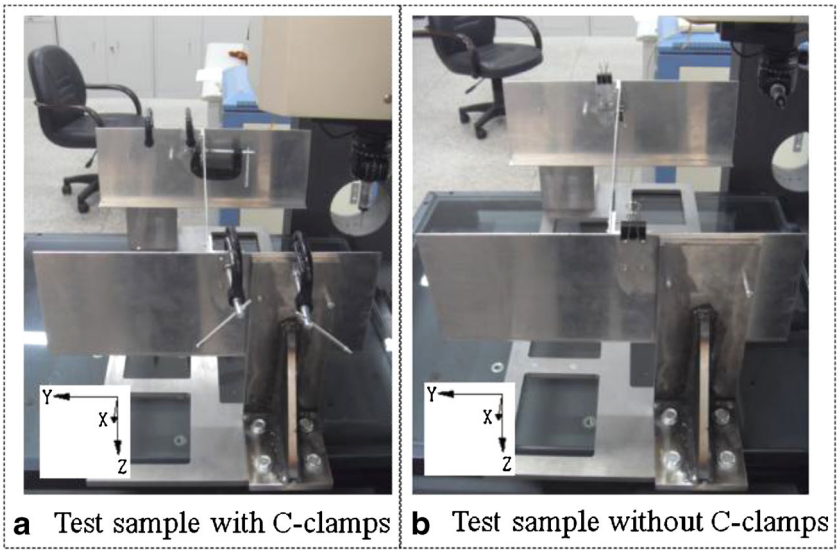


**Fig. 13** Two test samples and the coordinate system of CMM. **a** Test sample with C-clamps; **b** Test sample without C-clamps

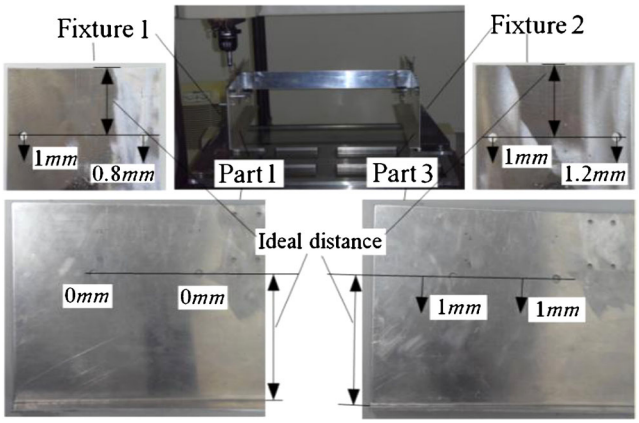


**Fig. 15** Deviated distance and direction of pin hole

The left chart in Fig. 9 shows the rotational and translational motions of Joint 1 and Part 1 located on Fixture 1, and the right one is the motions of Joint 2 and Part 3 located on Fixture 2. Intuitively, the motions in the left are more apparent than the right. Fortunately, the right can be found in Fig. 10.

Figure 10 illustrates the deformation of Part 2. It is induced by gaps from Joint 1 and Joint2. In the left side, a rotational displacement can be easily found. Actually, it is the compound of rotational and translational gaps in sequence Fixture 1, Part 1, and Joint 1. In the right side, the translational displacement can be found. It is the accumulated translational gaps in sequence Fixture 2, Part 3, and Joint 2.

In the right chart of Fig. 8, the maximum displacement magnitude (0.65 mm) is mainly induced by the gravity. In Fig. 11, the maximum displacement magnitude (5.5 mm) is the deformation that releases the gap-induced deformation in Fig. 10 to the entire assembly.

These figures emphasize the motion transfer mechanism in the simulation. This mechanism requires a stack up about the key point motions in related calculation steps for the actual key point motions.

## 5.2 Comparison validation between experiments and simulations

To present the practical prediction performance, two experiments are executed using parallel assembly. Feature and key points are, respectively, selected from the mating surfaces and assembly contour. Figure 12 shows the main dimensions and these point locations. As shown in Fig. 13, experiments contain two samples: one uses C-clamps and the other uses binder clips to replace C-clamps. The purpose of the two samples is to find the clamping effect in the assembly because the C-clamp is much heavy while the gravity of binder clip can be neglected. Figure 13 also represents the test coordinate system that is different from the GCS in the simulation.

### *5.2.1 The use of the additional points of the experimental sample*

Besides, coordinates of the points in Fig. 12, the other point coordinates are also measured, i.e., 6 points at the top surfaces

**Table 4** GCS coordinates and gaps of feature points for test sample with C-clamps (unit; mm)

| Name | Feature point | $x$ | $y$ | $z$ | $\delta x$ | $\delta y$ | $\delta z$ |
|---|---|---|---|---|---|---|---|
| Part 1 | $P_{11}$ | 122.5 | 245 | −90 | 0.1837 | 1.4421 | 1.3887 |
| | $P_{12}$ | 122.5 | 245 | −20 | 0.1154 | 0.9734 | 0.7478 |
| | $P_{13}$ | 122.5 | 225 | −20 | 0.112 | 0.9516 | 0.9971 |
| Joint 1 | $P_{21}$ | 126.5 | 240 | −111.7 | 0.4096 | 0.1028 | −0.387 |
| | $P_{22}$ | 126.5 | 218 | −111.7 | 0.3013 | 0.9395 | −0.3841 |
| | $P_{23}$ | 126.5 | 218 | −126.7 | 0.2676 | 1.3201 | 0.7227 |
| Part 2 | $P_{31}$ | 162.5 | 260 | −151.2 | −0.4181 | 1.1369 | 0.1649 |
| | $P_{32}$ | 162.5 | 245 | −151.2 | 0.0822 | 0.868 | 0.1791 |
| | $P_{33}$ | 132.5 | 245 | −151.2 | 0.5098 | 1.3505 | −0.0142 |
| | $P_{34}$ | 542.5 | 260 | −148.7 | −0.3796 | −0.0505 | −0.3884 |
| | $P_{35}$ | 542.5 | 245 | −148.7 | −0.3792 | 0.5483 | −0.6255 |
| | $P_{36}$ | 572.5 | 245 | −148.7 | 0.1544 | 0.8624 | −0.4825 |
| Joint 2 | $P_{41}$ | 578.5 | 240 | −188.2 | −0.4286 | 0.5441 | 0.2125 |
| | $P_{42}$ | 578.5 | 218 | −188.2 | −0.7096 | −0.7817 | −0.2993 |
| | $P_{43}$ | 578.5 | 218 | −173.2 | −0.6954 | −0.7812 | −1.0626 |
| Part 3 | $P_{51}$ | 582.5 | 245 | −210 | 0.0159 | −0.0801 | −0.1579 |
| | $P_{52}$ | 582.5 | 245 | −280 | 0.3038 | −0.0822 | −0.6147 |
| | $P_{53}$ | 582.5 | 225 | −280 | 0.2256 | −0.3182 | −0.613 |

**Table 5** GCS coordinates and gaps of feature points for test sample without C-clamp (unit; mm)

| Name | Feature point | $x$ | $y$ | $z$ | $\delta x$ | $\delta y$ | $\delta z$ |
|---|---|---|---|---|---|---|---|
| Part 1 | $P_{11}$ | 122.5 | 245 | −90 | −0.126 | 1.5397 | 0.5959 |
| | $P_{12}$ | 122.5 | 245 | −20 | 0.5344 | 1.5902 | 1.5633 |
| | $P_{13}$ | 122.5 | 225 | −20 | 0.515 | 1.3380 | 0.3853 |
| Joint 1 | $P_{21}$ | 126.5 | 240 | −111.7 | 0.187 | 0.2487 | 0.5415 |
| | $P_{22}$ | 126.5 | 218 | −111.7 | 0.3894 | 0.1500 | −0.1880 |
| | $P_{23}$ | 126.5 | 218 | −126.7 | 0.2182 | 0.1495 | −0.5878 |
| Part 2 | $P_{31}$ | 162.5 | 265 | −149.95 | 0.9470 | −1.3142 | −0.0463 |
| | $P_{32}$ | 162.5 | 215 | −149.95 | 0.0554 | −1.3141 | 1.5039 |
| | $P_{33}$ | 144.5 | 215 | −149.95 | 0.0546 | −1.1670 | 1.1457 |
| | $P_{34}$ | 542.5 | 265 | −149.95 | 0.1197 | 0.3564 | −0.2364 |
| | $P_{35}$ | 542.5 | 215 | −149.95 | 0.0665 | 0.5738 | 0.1480 |
| | $P_{36}$ | 560.5 | 215 | −149.95 | 0.0946 | 0.4161 | 0.2335 |
| Joint 2 | $P_{41}$ | 578.5 | 240 | −188.2 | 0.6755 | 0.0453 | −0.0772 |
| | $P_{42}$ | 578.5 | 218 | −188.2 | 0.1703 | 0.6913 | −0.1714 |
| | $P_{43}$ | 578.5 | 218 | −173.2 | 0.2790 | 0.6915 | −1.7530 |
| Part 3 | $P_{51}$ | 582.5 | 245 | −210 | −1.1871 | −0.5418 | 0.4607 |
| | $P_{52}$ | 582.5 | 245 | −280 | −0.8706 | 0.2068 | −0.1340 |
| | $P_{53}$ | 582.5 | 225 | −280 | −0.9792 | −0.6535 | −0.1363 |

of fixtures, locating points of each three feature points (Fig. 14), complement points of different probe poses of coordinate measurement machine (CMM), and the pin hole machining errors between fixture and part (Fig. 15).

- Assembly horizontality is corrected by the points on the fixture top surfaces.
- Mating gaps are computed from the vector subtraction of measured ***r*** in Fig. 14 to the ideal feature point vector.
- Complement points can be used to modify the tested coordinates to one unified coordinate system.
- Pin hole errors are used to correct the measured mating gaps.

*5.2.2 Feature point gaps in GCS*

Feature point gaps are yielded from the measured data. After the coordinate system conversion, Tables 4 and 5, respectively, give the GCS coordinates and gaps of feature points of test sample with or without C-clamps.

*5.2.3 The simulated 3D motion of the experimental sample*

Using the data in Tables 4 and 5, the proposed method will reach the global 3D motions of experimental samples. The gap-induced motions and the released motions are briefly represented in Figs. 16 and 17.

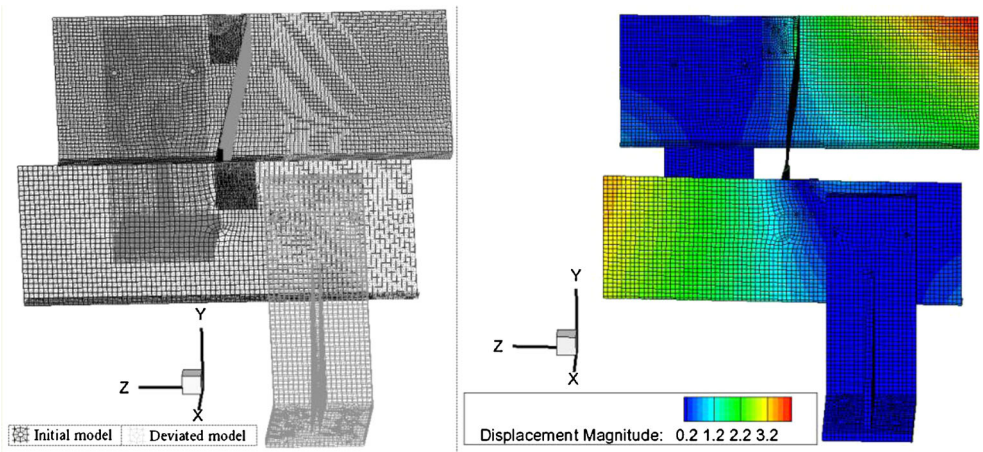


**Fig. 16** 3D motion of test sample with C-clamps (unit; mm)

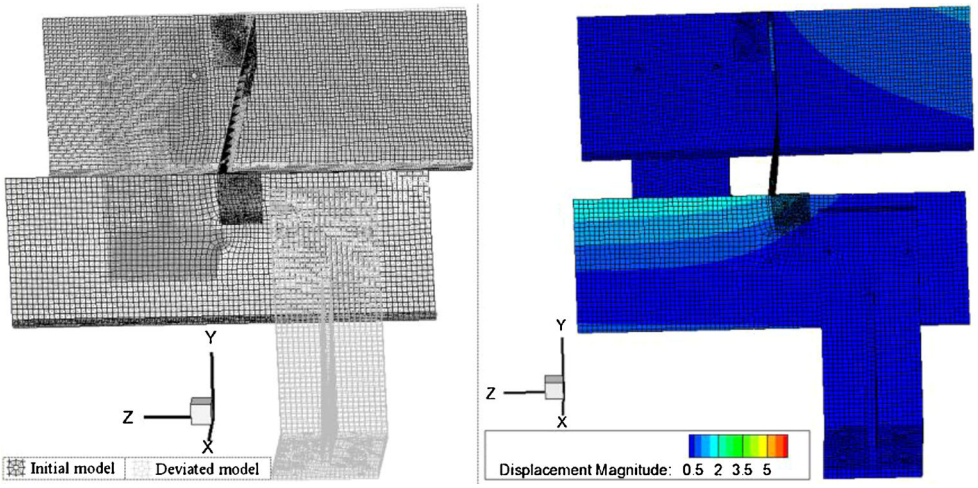


**Fig. 17** 3D motion of test sample without C-clamp (unit; mm)

### 5.2.4 Comparison between the simulation and experiment

Key point motion comparison between the simulation and the experiment is performed in the coordinate system of CMM. It comprises of 33 tested key points and 303 deviated FE nodes which are computed from the mating gaps of 18 feature points.

The deviated key points in the simulation result are firstly converted to test coordinate system using the tested locations of two points at the top fixture surfaces.

Then, the deviated test key point coordinates are converted to the same place of the simulated data by Lagrange interpolation using the measured pin hole error in Fig. 15. The final forms are directly given in Fig. 18.

### 5.2.5 Comparison discussion

Intuitively, Fig. 18b illustrates a better simulation result for the tested key point deviations than that in Fig. 18a.

In Fig. 18b, the biggest error is less than 0.5 mm. This error is caused by the geometric errors of the test sample and the statistical error of the proposed method. Because the experiment does not use C-clamp, and the simulation does not consider the gravity of C-clamps, the comparison effect is good.

In Fig. 18a, the biggest error is about 2 mm. Subtracting the geometric and method errors 0.5 mm, about 1.5 mm will be left for the error in Fig. 18a. The related regions of test sample and the deviated key points are shown in Fig. 19. There are six C-clamps on the sample in the left chart. C-clamp that is made by steel has a bigger density than the aluminum-made test sample. The four clamps near the regions (A and B) induce the drop-down of related dimensions along *Z*-axis. That is the growth along *Z*-axis of dimensions at regions A and B which are the sources for the distribution changing of the coordinates of tested key points in the right chart of Fig. 19. However, FE models do not consider the gravity of any clamp. Thus, the additional 1.5 mm error is yielded.

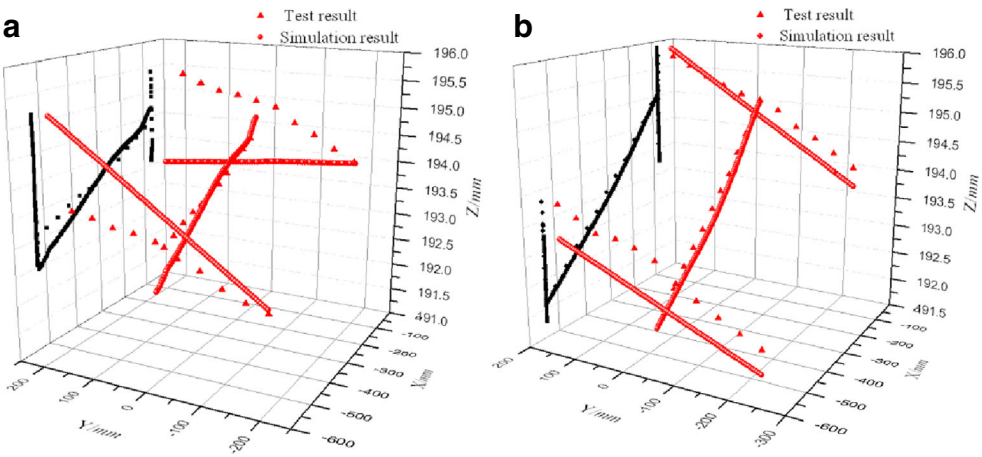


**Fig. 18** Result comparisons between tests and simulations (unit; mm). **a** Result comparison for the sample with C-clamps; **b** Result comparison for the sample without C-clamp

Result comparison for the sample with C-clamps

Result comparison for the sample without C-clamp

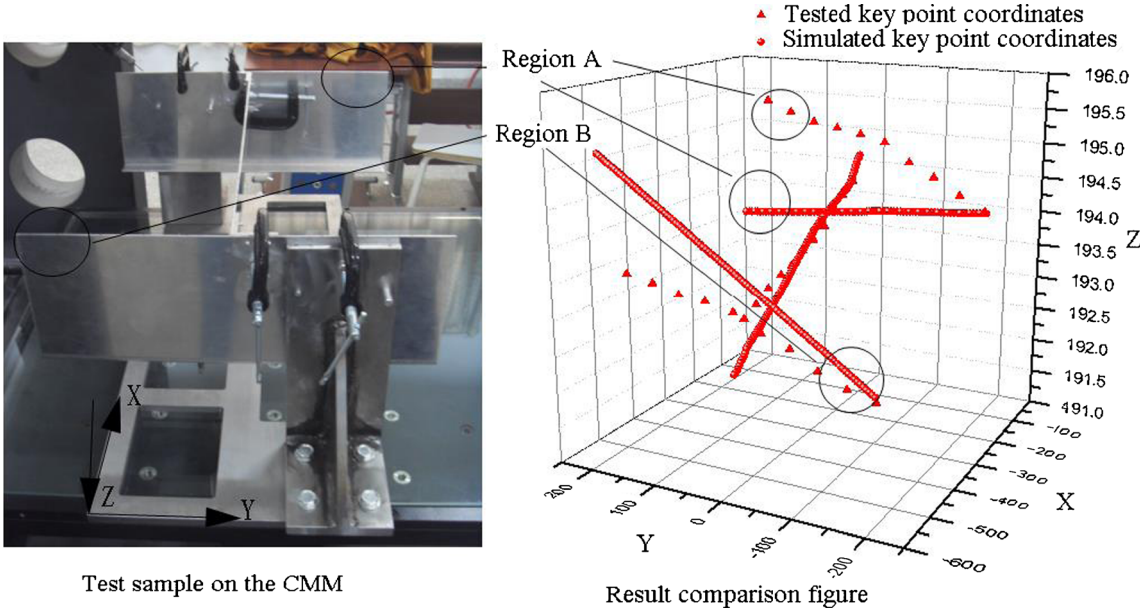


**Fig. 19** The spatial relation between the test sample contour and the key points in result comparison figure (unit; mm)

The proposed method does not consider the clamp-induced deformation due to the clamp-induced deformation will spring back when clamps are removed after the assembly. The spring-back can be validated by the comparison of Fig. 18b.

Because the 3D precision result error of a 460×400×257 mm test sample without C-clamp is less than 0.5 mm, the proposed method has enough precision for practice application.

## 6 Conclusion

This paper establishes the feasible kinematic formulations between the mating gaps and any point 3D rigid motion in sheet metals, and proposes an integrated 3D precision analysis method with rigid and compliant motions for sheet metal assembly. Hence, the comprehensive contour motions of sheet metals under the influence of mating gaps and gravities are solved. The proposed method is validated by the case studies of sequence and parallel assemblies.

Result comparisons suggest: (1) kinematic formulations which are yielded from the approximation of velocity to micro motion can accurately compute the gap-induced rigid motion; (2) 3D precision analysis approach is the integration of different types of codes which are handling the gap-induced rigid motion, gap-induced deformation, and gravity-induced deformation; (3) the proposed method has enough precision for engineering application based on the result comparison for the experimental sample without C-clamp.

In the future, two perspectives are focused. One is, for more complex assembly, the integration approach of the codes handling the gap-induced rigid motion, gap-induced deformation, and gravity-induced deformation. The other is an effective integration with the local deformations at the joints, which makes true the comprehensive dimensional precision analysis for further precision control and process optimization of sheet metal assemblies.

**Acknowledgments** This paper was financially supported by Certain Ministry of China (No. 51318010103, 51318010211, 51318010404, 9140A18010111JW0602) and National High Technology Research and Development Program of China (No. 2012AA040903).

## References

1. Blanchot V, Daidie A (2006) Riveted assembly modeling: Study and numerical characterisation of a riveting process. J Mater Process Technol 180:201–209
2. Saadat M, Cretin L, Sim R, Najafi F (2009) Deformation analysis of large aerospace components during assembly. Int J Adv Manuf Technol 41:145–155
3. Ruze J (1952) The effect of aperture errors on the antenna radiation pattern. II Nuovo Cimento 9(3 Supplement):364–380
4. Duan B (2002) Review of antenna structural design with mechatronics in China. Mechatronics 12:657–667
5. Chase KW, Greenwood WH (1988) Design issues in mechanical tolerance analysis. ASME Manuf Rev 1(1):50–59
6. Mazur M, Leary M, Subic A (2011) Computer aided tolerancing platform for the design of assemblies under external and internal forces. Comput Aided Des 43:707–719
7. Hu SJ (1997) Stream-of-variation theory for automotive body assembly. Ann CIRP 46:1–6
8. Liu SC, Hu JS (1997) Variation simulation for deformable sheet metal assemblies using finite element methods. J Manuf Sci Eng 119:368–374

9. Long Y (1998) CAVA manual. The University of Michigan, Ann Arbor
10. Cai W, Hu SJ, Yuan JX (1996) Deformable sheet metal fixturing: Principles, algorithms and simulations. ASME J Mech Des 118(3): 318–324
11. Cai W, Wang P, Yang W (2005) Assembly dimensional prediction for self-piercing riveted aluminum panels. Int J Mach Tools Manuf 45: 695–704
12. Cai W, Hsieh C, Long Y, Marin SP, Oh KP (2006) Digital panel assembly methodologies and applications for compliant sheet metals. ASME J Manuf Sci Eng 128:270–280
13. Dahlström S, Lindkvist L (2007) Variation simulation of sheet metal assemblies using the method of influence coefficients with contact modeling. J Manuf Sci Eng 129:615–622
14. Cai W, Hu SJ, Yuan JX (1997) A variational method of robust fixture configuration design for 3-D workpieces,". ASME J Manuf Sci Eng 119(4):593–602
15. Loose JP, Zhou S, Ceglarek D (2007) Kinematic analysis of dimensional variation propagation for multistage machining processes with general fixture layouts. IEEE Trans Autom Sci Eng 4(2):141–152
16. Jin J, Shi J (1999) State space modeling of sheet metal assembly for dimensional control. Trans ASME 121:756–761
17. Ceglarek D, Huang W, Zhou S, Ding Y, Ramesh K, Zhou Y (2004) Time-based competition in manufacturing: stream-of variation analysis (SOVA) methodology-review. Int J Flex Manuf Syst 16(1):11–44
18. Yue Y, Camelio J, Chin M, Cai W (2007) Product oriented sensitivity analysis for multi-station compliant assemblies. ASME J Mech Des 129(8):844–851
19. Cai W (2008) A new tolerance modeling and analysis methodology through a two-step linearization with applications in automotive body assembly. SME J Manuf Syst 27:26–35
20. Huang W, Lin J, Bezdecny MR, Kong Z, Ceglarek D (2007) Stream-of-variation modeling I: a generic 3D variation model for rigid body assembly in single station assembly processes. J Manuf Sci Eng 129(4):821–831
21. Huang W, Lin J, Kong Z, Ceglarek D (2007) Stream-of-variation (SOVA) modeling II: a generic 3D variation model for rigid body assembly in multi station assembly processes. J Manuf Sci Eng 129(4):832–842
22. Huang W, Kong Z (2008) Simulation and integration of geometric and rigid body kinematics errors for assembly variation analysis. J Manuf Syst 27:36–44
23. Wang H, Ceglarek D (2009) Variation propagation modeling and analysis at preliminary design phase for multi-station assembly systems. Assem Autom Int J Assem Technol Manag 29(2):154–166
24. Cheng H, Li Y, Zhang K, Mu W, Liu B (2011) Variation modeling of aeronautical thin-walled structures with multi-state riveting. J Manuf Syst 30(2):101–115
25. Cai W (2006) Robust pin layout design for sheet-panel locating. Int J Adv Manuf Technol 28:486–494
26. Ni J, Tang W, Xing Y (2013) Equivalent calculation of riveted assembly deformation and its application in assembly dimensional analysis. ASME J Manuf Sci Eng, in review
27. Chase KW, Magleby SP, Glancy CG (1998) A comprehensive system for computer-aided tolerance analysis of 2D and 3D mechanical assemblies. Geometric Design Tolerance, Theories, Standards and Applications. Chapman and Hall, London, pp 294–307